ACS chemical biology

Articles

pubs.acs.org/acschemicalbiology

# Inhibition of Biocatalysis in [Fe−Fe] Hydrogenase by Oxygen: Molecular Dynamics and Density Functional Theory Calculations

Gongyi Hong[†,‡] and Ruth Pachter*[,†]

[†]Air Force Research Laboratory, Wright-Patterson Air Force Base, Ohio 45433, United States

[‡]General Dynamics Information Technology, Inc., Dayton, Ohio 45433, United States

Supporting Information

**ABSTRACT:** Designing $O_2$-tolerant hydrogenases is a major challenge in applying [Fe−Fe]$H_2$ases for $H_2$ production. The inhibition involves transport of oxygen through the enzyme to the H-cluster, followed by binding and subsequent deactivation of the active site. To explore the nature of the oxygen diffusion channel for the hydrogenases from *Desulfovibrio desulfuricans* (*Dd*) and *Clostridium pasteurianum* (*Cp*), empirical molecular dynamics simulations were performed. The dynamic nature of the oxygen pathways in *Dd* and *Cp* was elucidated, and insight is provided, in part, into the experimental observation on the difference of oxygen inhibition in *Dd* and the hydrogenase from *Clostridium acetobutylicum* (*Ca*, assumed homologous to *Cp*). Further, to gain an understanding of the mechanism of oxygen inhibition of the [Fe−Fe]$H_2$ase, density functional theory calculations of model compounds composed of the H-cluster and proximate amino acids are reported. Confirmation of the experimentally based suppositions on inactivation by oxygen at the $[2Fe]_H$ domain is provided, validating the model compounds used and oxidation state assumptions, further explaining the mode of damage. This unified approach provides insight into oxygen diffusion in the enzyme, followed by deactivation at the H-cluster.

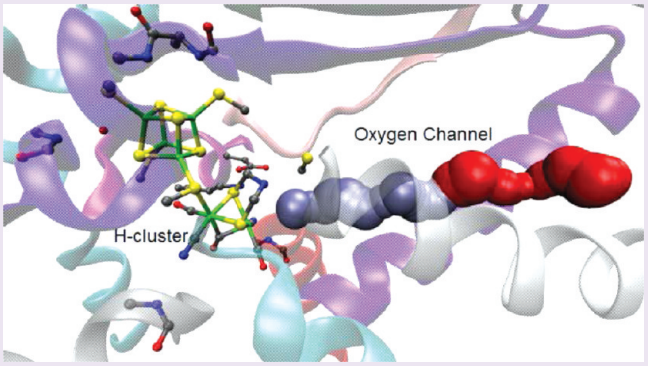


Hydrogen production is widespread among microorganisms, and photosynthetic candidates such as microalgae and cyanobacteria have been of great interest for that purpose.[1−3] [Fe−Fe] hydrogenases ([Fe−Fe]$H_2$ases) in particular were shown to have higher efficiency in hydrogen production, as compared to [Ni−Fe]$H_2$ases. The active site in the enzyme, also known as the H-cluster, contains a di-iron complex ($[2Fe]_H$ domain) and a proximal [4Fe-4S] cluster that is covalently linked to $[2Fe]_H$ by a protein cysteine thiolate group. However, [Fe−Fe]$H_2$ases are prone to irreversible damage by oxygen.[4] Efforts in unraveling the mechanism of $O_2$ inactivation for mitigation of the damaging response led to experimental[5−10] and theoretical[11−15] exploration of various aspects of the problem, however, as yet to be fully explained. For example, electrochemical analysis[5] demonstrated that inactivation proceeds by reversible formation of an oxygen adduct followed by irreversible transformation at the active site, namely, the H-cluster. Interestingly, the enzyme from *Clostridium acetobutylicum* (*Ca*) demonstrated less sensitivity to oxygen as compared to the [Fe−Fe]$H_2$ase from *Desulfovibrio desulfuricans* (*Dd*), as reported by Baffert *et al.*[5] and confirmed by Liebgott *et al.*[6] The higher rate of inhibition by oxygen in *Dd*, as compared to *Ca*, for which no X-ray crystal structure was determined but which is assumed to be highly similar to the enzyme from *Clostridium pasteurianum* (*Cp*),[8] has indeed been pointed out as puzzling,[7] and the disparity is unclear due to the similarity of the H-cluster in both enzymes.

First, the oxygen diffusion channels to the active site have to be considered. Because engineering the [Fe−Fe]$H_2$ase to slow the oxygen access to the H-cluster may decrease its inhibition, the presumed dependence on the oxygen diffusion channels was explored, for example, by Lautier *et al.*[8] Three putative pathways that extend from the solvent to the active site of the [Fe−Fe] hydrogenase and so-called central cavity C leading to the active site were suggested. Channel A, which was originally discovered by Fontecilla and co-workers,[16] comprises an elongated cavity extending from the protein surface to cavity C. Channel B, so-called dynamic, which was identified by molecular dynamics (MD) simulations, was previously suggested to be the dominant route for oxygen transport.[17] Channel W is lined by hydrophilic amino acids that stabilize water molecules.

Relative positioning of the possible oxygen diffusion channels in *Cp* based on the X-ray structure[18] are illustrated in Figure 1a, as well as some of the amino acids along pathways A and C (Figure 1b). Notably, the amino acids that comprise cavity C are conserved in the hydrogenases that were analyzed,[8] but this

Received: March 13, 2012
Accepted: April 30, 2012
Published: May 7, 2012

  

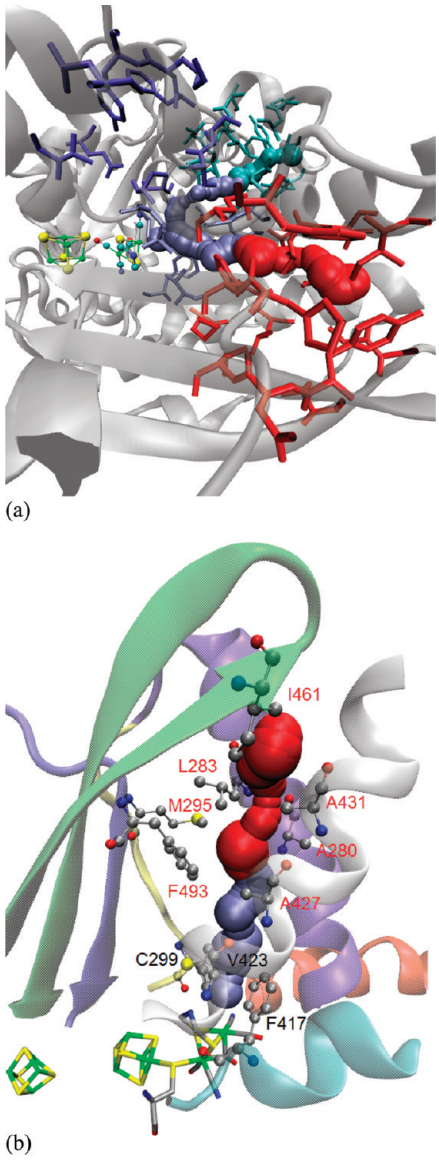


**Figure 1.** Analysis of the *Cp* X-ray structure for (a) channels A (red), B (cyan), C (ice blue), and W (violet), as derived by MolAxis[24] and (b) details of amino acids around channels A and C.

is not the case for pathways A and B. Thus, cavity C may not explain the difference in activity inhibition by oxygen between *Dd* and *Ca*. King *et al.*[19] have shown that mutation in the enzyme from *Chlamydomonas reinhardtii* (*Cr*), specifically of Val to the bulkier Trp for the amino acid equivalent to Val423 in *Cp*, has increased its oxygen tolerance. Efforts in mutating amino acids along the presumed A and C paths in *Ca* were mostly unsuccessful,[8] except for one case (A426L). However, the relevant amino acid is the same in *Dd* and *Cp* in this case and therefore does not explain the different behavior. Moreover, theoretical work in comparing the putative pathways in the enzymes has been limited.

Next, the mechanism of oxygen inactivation at the active site is of interest. This was examined for *Cr* by Stripp *et al.*,[9] including by X-ray absorption spectroscopy, postulating that $O_2$ binds first at the $[2Fe]_H$ domain, forming a reactive oxygen species (ROS) that subsequently either migrates and attacks the [4Fe-4S] cluster (so-called mechanism A) or remains bound at $Fe_d$, exerting long-range oxidation by electron transfer (so-called mechanism B).[9] In either case it is likely that the H-cluster is at oxidation level $H_{ox}$ because of EPR evidence that CO binds preferentially in this oxidation state.[20] The supposition of a three-stage mechanism was further confirmed by an X-ray absorption spectroscopy study of *Cr* reported by Lambertz *et al.*,[10] using a time-resolved approach, where three apparent kinetic phases were deduced, namely, the formation of a ROS at the active site, ROS attack of the [4Fe-4S] cluster, and complete oxygen-induced degradation. Note that regarding the $O_2$-induced damage of the $[4Fe\text{-}4S]^{2+}$ cluster, the aerobically purified hydrogenase from *Desulfovibrio vulgaris* (*Dv*, having the same amino acid sequence as *Dd*) was shown by EPR to exhibit an intense signal indicative of a $[3Fe\text{-}4S]^{+}$ cluster, accounting for up to 0.2 spin/molecule, dependent on the preparation conditions. This signal is attributed to a $[3Fe\text{-}4S]^{+}$ impurity resulting from oxidative damage.[21]

In this work, to explain in part the experimental observation on the difference of oxygen inhibition in *Dd* and *Ca* (assumed homologues to *Cp*), comprehensive empirical MD simulations were undertaken. The dynamic nature of the oxygen pathways in *Dd* and *Cp* was elucidated, and non-conservation of the sequence in channel A was considered. Such an approach was taken for design of oxygen tolerance in a [NiFe] hydrogenase.[22] As the oxygen proceeds to cavity C and the active site, density functional theory (DFT) calculations for model compounds of the *Cp* $[Fe\text{–}Fe]H_2$ase provided insight into details of the inactivation. To discern the effect of the most proximate amino acid in cavity C to the H-cluster, Cys299 was included in the model compounds, which is also at the origin of the proton channel,[23] as well as other relevant aspects of the protein environment. Further confirmation of the experimentally based suppositions on inactivation by oxygen at the $[2Fe]_H$ domain was provided, as well as validation of the model compounds used and oxidation state assumptions. This unified approach provides insight into the transport of oxygen through the enzyme, followed by deactivation at the H-cluster.

## RESULTS AND DISCUSSION

**Oxygen Diffusion in *Cp* and *Dd*.** Cavity C and diffusion channel A were analyzed on the basis of 40 ns trajectories from MD simulations at 300 K, based on fully equilibrated systems, derived from the *n*th ns frame for each enzyme. The oxygen diffusion pathways were identified and characterized by using the program MolAxis.[24] The MolAxis algorithm relies on alpha shapes and a medial axis, namely, the collection of 3D points that have more than one closest point on the surface, which is the van der Waals surface of the atoms in this case.[24] The bottleneck radius of a channel was defined by its smallest radius. Bottleneck radii (BNR) *versus* MD simulation time for *Dd* and *Cp* for cavity C and channel A are shown in Figure 2a and b, respectively.

Relatively large variations in the BNR are noted between the two enzymes for cavity C (see Figure 2a). In particular, BNR of 1.12 Å for *Cp* and 1.11 Å for *Dd* in the X-ray crystal structures were modified to average values of 0.74 and 1.07 Å, respectively, when a realistic environment was considered in the simulations. Smaller changes were noted correspondingly for channel A (Figure 2b), where the BNR changed from *Cp* = 0.89 Å, *Dd* = 1.05 Å in the X-ray structures to average values of *Cp* = 0.93 Å, *Dd* = 0.98 Å, respectively, as derived from the simulations. However, the trend of a smaller BNR for *Cp* remained consistent. Interestingly, the relatively smaller BNR for *Cp* are consistent with the experimental result that *Dd* has a


dx.doi.org/10.1021/cb3001149 | *ACS Chem. Biol.* 2012, 7, 1268–1275

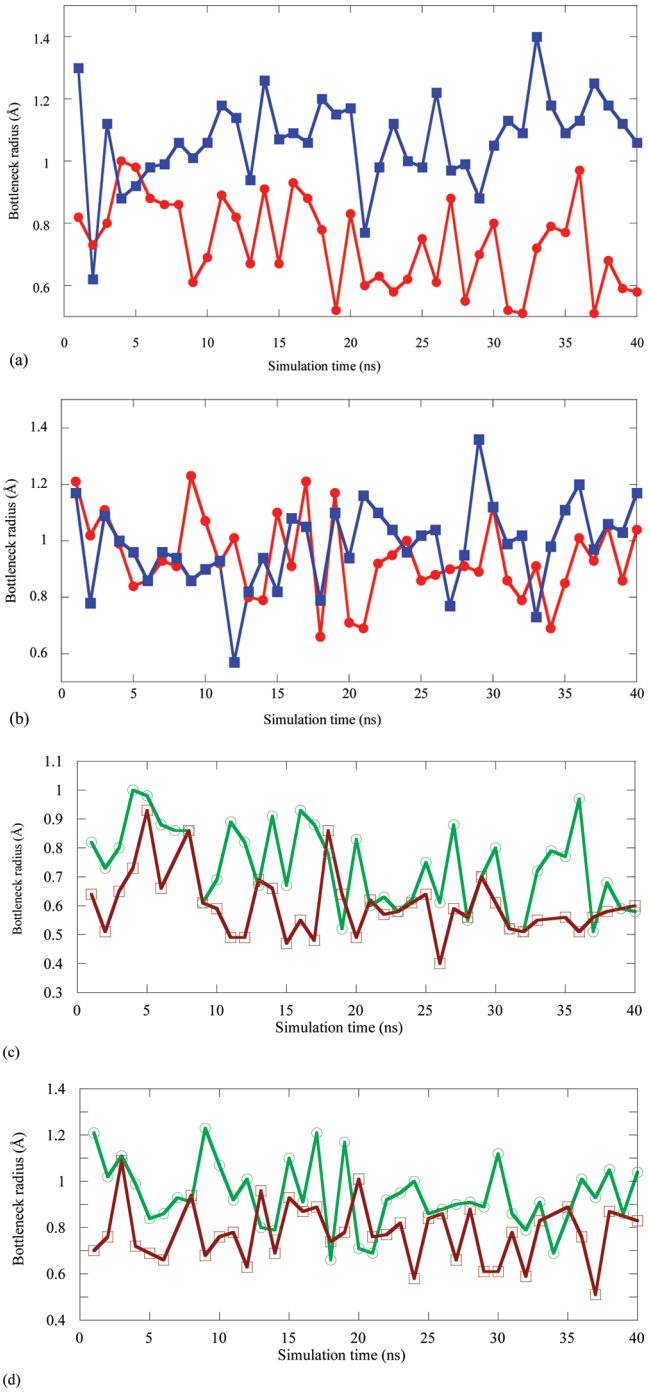


**Figure 2.** BNR derived from MD simulations *versus* simulation time for *Dd* (blue filled squares) and *Cp* (red filled circles) for (a) cavity C and (b) channel A. Comparison of BNR for *Cp* in (c) pathways C and A (green open circles) and C and B (brown open squares) and (d) pathways A (green open circles) and B (brown open squares).

higher rate of inhibition by oxygen than *Ca*,[8] which is highly homologous to *Cp*.

To examine in more detail changes in the BNR during the MD simulation, three structures from the *Cp* simulation trajectories were chosen, specifically the 4th ns structure with a BNR value of 1.00 Å, the 36th ns protein structure with a BNR of 0.97 Å, and the 37th ns structure with a BNR of 0.51 Å. Cavity C and diffusion channel A for *Cp*'s 36th and 37th structures are shown as an example in Figure 3. The dynamic

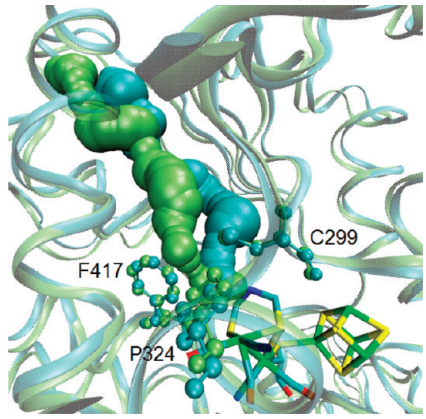


**Figure 3.** Comparison of channels C and A in *Cp* for the 36th ns MD selected trajectory (cyan) *versus* the 37th ns frame (lime).

nature of the bottleneck is demonstrated, confined by S(Cys299), $C_{\varepsilon 2}$(Phe417), and $N_S$(DTMA) in the 36th structure and by S(Cys299), $C_\gamma$(Pro324), and $C_{\varepsilon 2}$(Phe417) in the 37th structure (rmsd value of the backbone for the channel was 0.45 Å, while the corresponding value in comparing the 4th and 37th ns protein structures was 0.72 Å). Notably, the bottleneck radius of cavity C derived from the 40th structure was 0.58 Å for *Cp* and 1.06 Å for *Dd*, confined by S(Cys299), $C_\gamma$(Pro324), and $C_{\varepsilon 2}$(Phe417) in *Cp* and by $C_\beta$ (Cys178), $C_\beta$(Pro203), and $C_{\varepsilon 2}$ (Phe296) in *Dd*, respectively (alignments of amino acids in *Cp* and *Dd* are listed in Supplementary Table 1S). Superposition of cavity C in *Cp* and *Dd* using the X-ray coordinates and the 40th ns MD trajectory is shown in Figure 4. Clearly, a larger deviation was noted in the MD simulation trajectories, compared to the X-ray structures, noting that in the 40th ns frame the thiol group in *Cp* rotated toward Pro324 and Phe 417, resulting in a smaller BNR. The smaller BNR in *Cp* than in *Dd* could be due to differences in spatial rearrangements in a highly dynamic environment.

To assess the viability of pathway B *versus* A for oxygen transport, BNR in *Cp* for pathways C and A, C and B, and A and B were examined, as shown in Figure 2c and d, respectively. In both cases the average BNRs are smaller when considering the C and B pathway as the oxygen diffusion channel, where for cavity C the values were 0.74 and 0.60 Å for C and A and for C and B, respectively, whereas for channels A and B the respective values were 0.94 and 0.77 Å. It seems that the oxygen pathway is governed by channel A and cavity C, contrary to a previous suggestion that the transient B pathway consists the dominant route for oxygen diffusion in the *Cp* hydrogenase.[17] Indeed, the A426L variant of *Cr* (corresponding to A427 in *Cp*) was reported to reduce the rate of $O_2$ binding,[8] implying that channel A is the dominant pathway in comparison to channel B.

In *Cr*, by mutating to more bulky amino acids along the pathways, mutations I460F and A430I (corresponding to I461F and A431I in *Cp*) were expected to obstruct channel A, while V422W and F416W (corresponding to V423W and F417W in *Cp*) were expected to obstruct cavity C, yet reduction in the rate of oxygen inactivation was not observed.[8] I461 is near the protein surface (see Figure 1b), while A431 is positioned around the bottleneck, and the side chain is pointing toward the channel. Failure of A431I to reduce $O_2$'s access could result, in part, from the dynamic nature of the oxygen pathways. On


dx.doi.org/10.1021/cb3001149 | *ACS Chem. Biol.* 2012, 7, 1268–1275

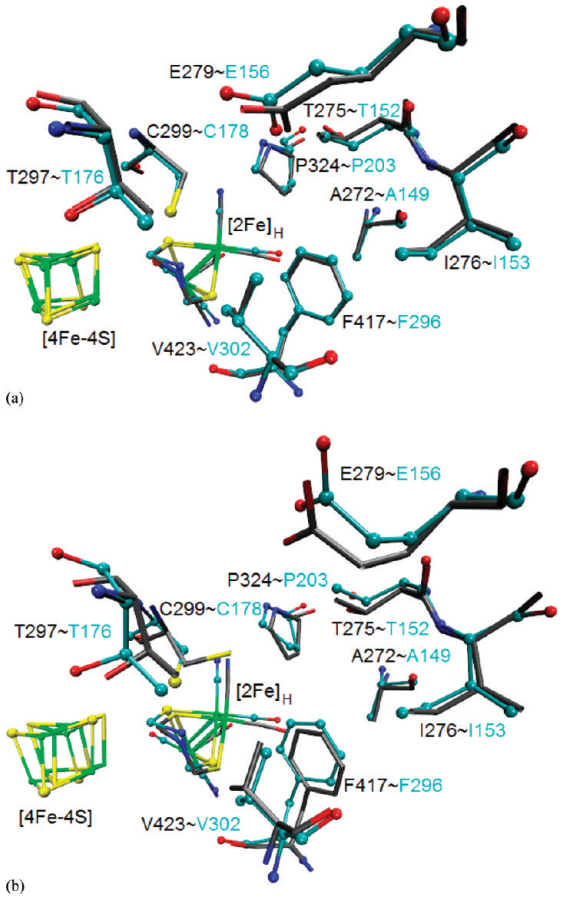


**Figure 4.** Alignment of cavity C and H cluster in *Cp* (gray, opaque bond form) and *Dd* (cyan, opaque CPK form) using (a) X-ray coordinates and (b) the 40th ns frame from the MD simulation trajectories.

the other hand, the A426L mutation in *Cr* was successful in improving oxygen inactivation.

In comparing *Cp*→*Dd*, we note that eight amino acids are different in the two proteins for channel A, namely, A280→G157, L283→F160, I287→L164, F293→L172, M295→Q174, I461→V340, Y466→V345, and N467→K346, respectively (shown in Supplementary Table 1S). The existence of somewhat bulkier amino acids for *Cp* than for *Dd* are noted overall, which is consistent with the calculated BNR from the MD simulations. In addition to a mutation of *Dd* to be consistent with the *Cp* primary structure for validation of this supposition (V340I), mutations that may strengthen or cause hydrogen bonding could be considered.

Lastly, note that presumably it is possible that water molecules are displaced by oxygen molecules in pathway W, although it is not postulated as a channel for oxygen transport. It was interesting to note that water diffusion through pathway W was observed during the MD simulations of *Cp*. Shown in Figure 5 are the trajectories of water612 located between C299 and E279 that is diffusing from cavity C into the bulk and of a water molecule that is diffusing from the bulk into cavity C in between C299 and E279, where both are passing along pathway W. C299 and E279 also play a role in proton transfer, as we have previously discussed.[23] The dynamical nature and interplay of the processes that occur in hydrogen production by the [Fe−Fe] hydrogenases require further analysis, to be carried out in future work.

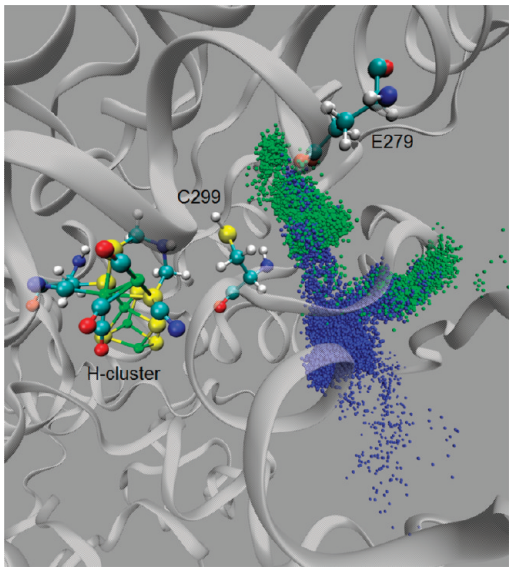


**Figure 5.** Trajectory of water612 initially located between C299 and E279 that diffused into the bulk (in green) and the trajectory of a water molecule initially in the bulk that moved in between C299 and E279 (in blue), transported along pathway W.

**Oxygen Inactivation at the H-Cluster.** To investigate theoretically the effects of oxygen binding at the H-cluster, once it passed through the diffusion channel, a few model compounds were considered, as shown in Figure 6. Model compound **1** consists of the H-cluster, four $S^{-}CH_3$ groups, side chain of Lys358, two backbone CONH groups (Pro231−Ser232, Pro324−Gln325) that form hydrogen bonds with $CN^{-}$ groups of the cluster, and the side chain of Glu361 that non-covalently binds to Lys358. Model compound **2** is an extension of **1** by including one water molecule from the *Cp* crystal structure (HOH585 in the PDB file 3C8Y) in the vicinity of the [4Fe-4S] cluster. Model compound **3** is an extension of **2** by inclusion of three backbone CONH groups (G506−G507, Met497−Ala498, Ala498−Cys499) that are located in the vicinity of the [4Fe-4S] cluster and the side chain of Cys299. End carbon atoms in the QM region (such as C of $S^{-}CH_3$) were fixed in the geometry optimization to mimic the protein environment's constrains, adding hydrogen atoms to saturate the valence of the carbon.

Analysis of our MD simulation trajectories of the *Cp* protein environment around the H-cluster has shown that the backbone CONH groups surrounding it did not fluctuate significantly. For example, structural alignment between the X-ray structure and 40th ns MD snapshot of the protein environment within 6 Å of the [4Fe-4S] cluster resulted in a rmsd value of 0.23 Å. In this respect, the model compounds considered are assumed to mimic reality reasonably well. Parts of the protein environment modeled were not included previously,[14] which may account for subtle effects not studied hitherto.

Experimentally it has been proposed that oxygen binds at $Fe_d$.[10] To validate this assumption and also the application of the model compounds we considered, we examined binding of $O_2$ either at $Fe_d$ of the $[2Fe]_H$ cluster or at the Fe atom of the [4Fe-4S] cluster closest to the water molecule included (so-called $Fe_4$, see Figure 6a). Selected geometrical parameters of the optimized structure of model compound **1** in the $H_{ox}$ oxidation state upon oxygen binding are shown in Figure 7.


dx.doi.org/10.1021/cb3001149 | *ACS Chem. Biol.* 2012, 7, 1268−1275

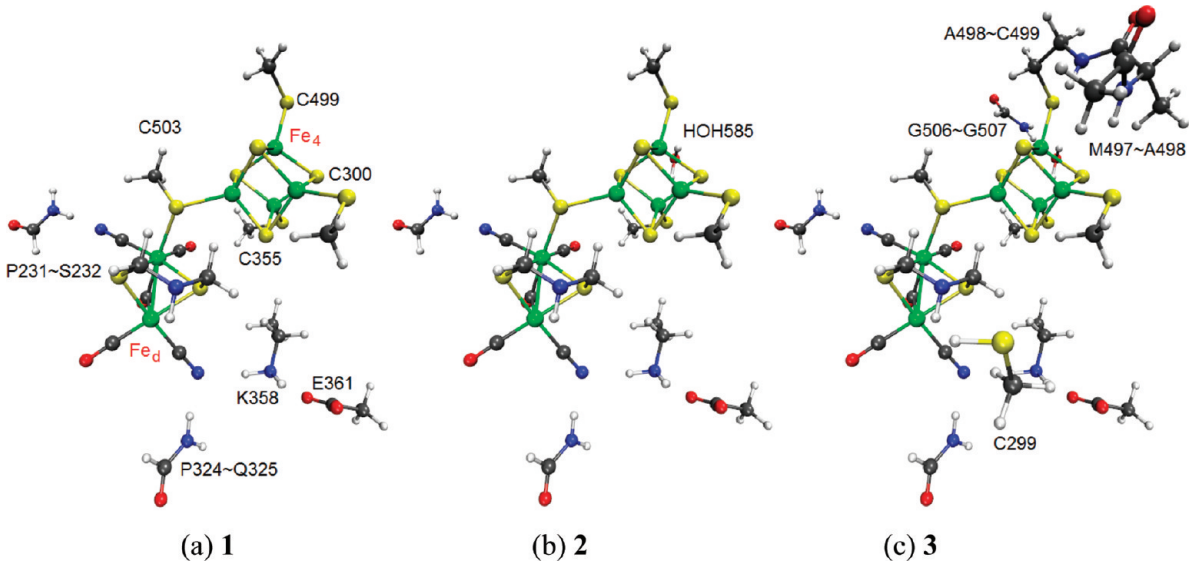


**Figure 6.** Model compounds **1** (a), **2** (b), and **3** (c) taken from the *Cp* X-ray structure.

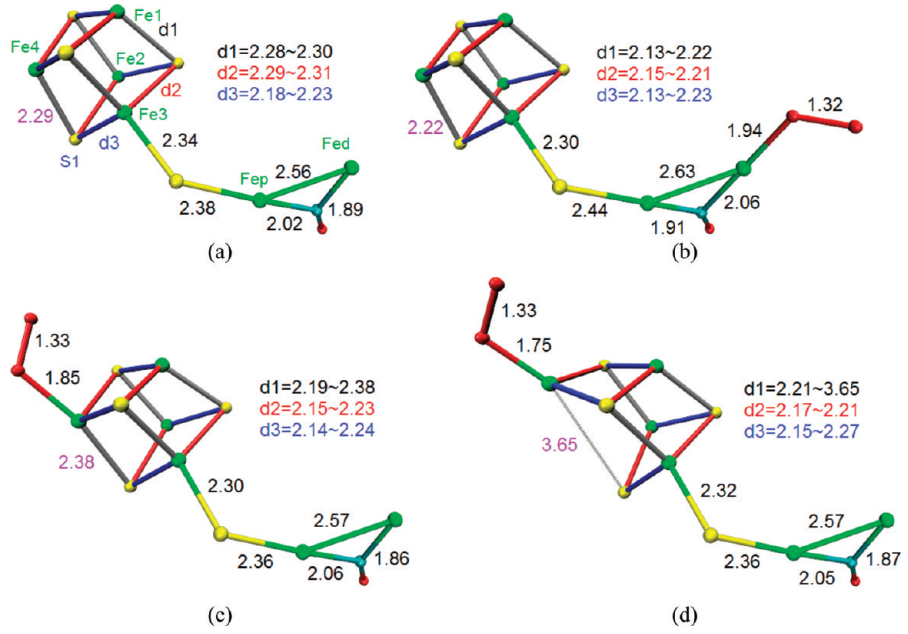


**Figure 7.** Geometrical parameters of optimized structures of model compound **1** in the $H_{ox}$ oxidation state (a) and after oxygen binding at $Fe_d$ (b) and $Fe_4$ (intact, c, distorted, d), respectively.

Changes in the geometry of the H-cluster's framework depend on the site of oxygen binding, and variations are noted accordingly in Figure 7b as compared to Figure 7c and d, as well as being listed in Table 1. Changes upon binding at a distorted [4Fe-4S] cluster to mimic potential binding at a partially disintegrated cluster as the deactivation process continues are shown in Table 1. Binding of oxygen at $Fe_d$ moves the $\mu$-CO toward $Fe_p$, increasing the $Fe_p$-S(Cys-bridging) distance by ~0.05 Å for $H_{ox}$ and by 0.32 Å for $H_{red}$. The reduced form of the H-cluster demonstrated smaller effects at [4Fe-4S] upon oxygen binding compared to $H_{ox}$ (Table 1), but larger deviations for $[2Fe]_H$. Such a change for the reduced form of the H-cluster was reported for CO binding at $Fe_d$ using DFT calculations.[15]

Binding of oxygen at $Fe_d$ lengthened the Fe−Fe distance in $[2Fe]_H$ by around 0.05 Å, whereas binding of oxygen at $Fe_4$ shortened Fe−Fe distances in $[2Fe]_H$. This result is consistent with the recent experimental observation that in the first phase of oxygen inactivation, the Fe−Fe distance in the $[2Fe]_H$ domain was lengthened, and the elongation was reversed in the later stage of the oxygen inactivation process.[10] The validity of the model compounds we used is therefore further confirmed. Although effects of the protein were shown to be relatively small in comparing compounds **1** and **3** (Table 1), especially for oxygen binding at $Fe_d$, the proximate water molecule stabilized the distorted [4Fe-4S] cluster, providing an understanding of possible effects of the environment.

We also note that the O−O distance upon binding is lengthened by ca. 0.1 Å, of 1.32−1.44 Å, as compared to the O−O distance (1.23 Å) of $O_2$, and close to the optimized O−O distance (1.37 Å) of superoxide.[25] Notably, the Mulliken atomic partial charges of the oxygen species (listed in


dx.doi.org/10.1021/cb3001149 | *ACS Chem. Biol.* 2012, 7, 1268−1275

**Table 1. Selected Distances (Å) of Optimized Structures of Model Compounds of the H-Cluster with and without Binding Oxygen Species**

| | $Fe_p$–$Fe_d$ | Fe–O | O–O | $Fe_p$–CO | $Fe_d$–CO | $Fe_p$–$SC_{503}$ | $Fe_3$–$SC_{503}$ | $Fe_4$–$S_1$ |
|---|---|---|---|---|---|---|---|---|
| **1** $H_{ox}$ | 2.56 | | | 2.02 | 1.89 | 2.38 | 2.34 | 2.29 |
| **1** $H_{ox}OO(Fe_d)$ | 2.63 | 1.94 | 1.32 | 1.91 | 2.06 | 2.44 | 2.30 | 2.22 |
| **1** $H_{ox}OO(Fe_4)^a$ | 2.57 | 1.85 | 1.33 | 2.06 | 1.86 | 2.36 | 2.30 | 2.38 |
| **1** $H_{ox}OO(Fe_4)^b$ | 2.57 | 1.75 | 1.33 | 2.05 | 1.87 | 2.36 | 2.32 | 3.65 |
| **1** $H_{red}$ | 2.68 | | | 2.89 | 1.76 | 2.30 | 2.24 | 2.14 |
| **1** $H_{red}OO(Fe_d)$ | 2.70 | 1.98 | 1.34 | 1.91 | 2.03 | 2.62 | 2.32 | 2.22 |
| **1** $H_{red}OO(Fe_4)^a$ | 2.61 | 1.91 | 1.33 | 2.18 | 1.81 | 2.39 | 2.26 | 2.34 |
| **1** $H_{red}OO(Fe_4)^b$ | 2.61 | 1.75 | 1.34 | 2.20 | 1.81 | 2.37 | 2.32 | 3.53 |
| **2** $H_{ox}$ | 2.58 | | | 2.06 | 1.86 | 2.38 | 2.30 | 2.21 |
| **2** $H_{ox}OO(Fe_d)$ | 2.62 | 1.93 | 1.32 | 1.91 | 2.06 | 2.43 | 2.30 | 2.21 |
| **2** $H_{ox}OO(Fe_4)^a$ | 2.57 | 1.90 | 1.32 | 2.07 | 1.86 | 2.34 | 2.26 | 2.36 |
| **2** $H_{ox}OO(Fe_4)^b$ | 2.56 | 1.84 | 1.43 | 2.02 | 1.89 | 2.35 | 2.32 | 4.01 |
| **3** $H_{ox}$ | 2.55 | | | 2.03 | 1.88 | 2.35 | 2.33 | 2.29 |
| **3** $H_{ox}OO(Fe_d)$ | 2.60 | 1.92 | 1.32 | 1.91 | 2.06 | 2.41 | 2.30 | 2.20 |
| **3** $H_{ox}OO(Fe_4)^a$ | 2.55 | 1.90 | 1.44 | 2.03 | 1.88 | 2.32 | 2.27 | 2.37 |
| **3** $H_{ox}OO(Fe_4)^b$ | 2.55 | 1.63 | 2.82 | 2.04 | 1.88 | 2.33 | 2.31 | 4.34 |

[a][4Fe-4S] cluster intact. [b][4Fe-4S] cluster distorted.

Supplementary Table 2S) are also consistent with preferred binding at $Fe_d$, showing larger partial atomic charges, of ca. −0.4e. Upon binding at the distorted [4Fe-4S] cluster, the values increase to about −0.6−0.8e, confirming continual disintegration of the cluster. It was shown theoretically that mutation of amino acids close to $Fe_d$ may inhibit oxygen binding.[13]

Further confirmation of the supposition of oxygen binding at $Fe_d$ was provided by the calculated binding energies (defined by $E$[H-cluster+$O_2$]-$E$[H-cluster]-$E$[$O_2$]), as listed in Table 2.

**Table 2. Binding Energies (kcal/mol) of $O_2$ at the H-Cluster**

| | binding energy at $Fe_d$ | binding energy at $Fe_4$ |
|---|---|---|
| **1** $H_{ox}$ ($H_{red}$) | −19.4 (−20.5) | −4.4;[a] −3.0;[b] (14.7;[a] −15.9[b]) |
| **2** $H_{ox}$ | −19.7 | −7.0;[a] −11.4[b] |
| **3** $H_{ox}$ | −16.1 | −4.1;[a] −29.2[b] |

[a][4Fe-4S] cluster intact. [b][4Fe-4S] cluster distorted.

Binding energies for **1**, **2**, and **3** for $H_{ox}$ are larger for $Fe_d$ than for $Fe_4$ binding, while it seems possible that after inactivation has already started additional oxygen molecules may directly bind at the [4Fe-4S] cluster until final destruction. Removing Cys299 from the $[2Fe]_H$ domain was found to have a small effect on the binding, consistent with the result that C298L and C298A in *Cr* (corresponding to C299 in *Cp*) variants had $O_2$ tolerance similar to that of the wild-type enzyme. The binding energy at the H-cluster in the $H_{red}$ oxidation state of −20.5 kcal/mol (Table 2), which was considered for comparison, was larger compared to the results for $H_{ox}$, which is consistent with previous computational work.[14]

In addition, compounds **1** and **3** were re-optimized with a distorted [4Fe-4S] cluster at the $H_{ox}$ oxidation state, where the oxygen is adsorbed at $Fe_d$, resulting in a recovery of the original [4Fe-4S] cluster geometry. This may support, in part, the experimental supposition that mechanism A rather than B is responsible for oxygen inactivation,[9,10] because after a superoxide is formed at $Fe_d$, a distorted cubane is not stable and direct destruction of the [4Fe-4S] cluster through long-range oxidation may not be favorable.

In summary, our MD simulations and DFT calculations provided insight into oxygen diffusion in the enzyme, followed by deactivation at the H-cluster. It was shown by the MD simulations that putative channel A can be assumed to be the oxygen channel carrier in *Cp* and *Dd*. The oxygen diffusion channel was analyzed in terms of bottleneck radii, demonstrating its dynamic nature. Moreover, the detailed BNR analysis demonstrated implied consistency with experimental data on oxygen inactivation in *Ca* and *Dd*. Finally, the detailed DFT calculations for complex model compounds, including the protein environment as much as possible, and analysis of the effects of oxygen binding on the structural parameters provided complementary understanding of the behavior at the active site, once the oxygen reached it after diffusing through the protein.

## METHODS

MD simulations were performed with Gromacs[26] (version 4.5.4) using the CHARMM force field,[27] where the coordinates of the H-cluster were fixed. X-ray structures of *Cp* and *Dd* were used as starting configurations, namely, PDB 3C8Y,[18] where the dithiomethylether ligand in $[2Fe]_H$ domain was replaced with dithiomethylamine, and similarly for PDB 1HFE,[16] respectively, which was also rationalized by simulation.[28] The proteins were embedded in a water box, using periodic boundary conditions, with 29081 (15844) CHARMM TIPS3P water molecules. Fourteen (7) randomly chosen water molecules were replaced with sodium ions to neutralize the *Cp* (*Dd*) proteins that include charged amino acids. A cutoff of 1.2 nm was used for the 12-6 Lennard-Jones potential calculations. For efficient modeling of electrostatics, particle-mesh Ewald sums were applied, with a short-range cutoff of 1 nm, and a relative strength of the Ewald-shifted direct potential of $10^{-5}$ at 1 nm (grid spacing of 0.12 nm, interpolation order of 6). The LINCS algorithm reset bonds to their correct lengths after an unconstrained update.[29] The system was equilibrated at constant temperature (300 K) and volume for 1 ns. Velocity rescaling with a stochastic term of 0.1 ps was used to regulate the temperature. On the basis of selected trajectories from the 40 ns simulation, oxygen pathways were derived using MolAxis.[24] TM-align[30] was used for superposition of protein structures and VMD[31] for visualization.

For model compounds of the H-cluster, unrestricted spin calculations were performed at the BP86[32,33]/6-31+G* level, using Gaussian 09.[34] The BP86 exchange-correlation functional was previously found to be adequate in this case.[11] The oxidation state of the active site was assumed $H_{ox}$ (charge of H-cluster = −3), with the


dx.doi.org/10.1021/cb3001149 | ACS Chem. Biol. 2012, 7, 1268–1275

[4Fe-4S] cluster in the +2 oxidation state. Four $S^{-}CH_3$ groups were included in the [4Fe-4S] model, and molecular oxygen was in the triplet ground state. Partial atomic charges were assigned using the ESP method.[35]

## ■ ASSOCIATED CONTENT

### Supporting Information

Partial alignment of amino acids that line cavity C and channel A in *Cp* and *Dd* and Mulliken partial atomic charges on oxygen species. This material is available free of charge *via* the Internet at http://pubs.acs.org.

## ■ AUTHOR INFORMATION


### Corresponding Author

*E-mail: Ruth.Pachter@wpafb.af.mil.


### Notes

The authors declare no competing financial interest.

## ■ ACKNOWLEDGMENTS

We gratefully acknowledge support from the Air Force Office of Scientific Research and helpful assistance from the AFRL DSRC for High Performance Computing.

## ■ REFERENCES


(1) Frey, M. (2002) Hydrogenases: Hydrogen-activating enzymes. *ChemBioChem 3*, 153−160.

(2) Vincent, K. A., Parkin, A., and Armstrong, F. A. (2007) Investigating and exploiting the electrocatalytic properties of hydrogenases. *Chem. Rev. 107*, 4366−4413.

(3) Stripp, S. T., and Happe, T. (2009) How algae produce hydrogen-news from the photosynthetic hydrogenase. *Dalton Trans.*, 9960−9969.

(4) Imlay, J. A. (2006) Iron-sulphur clusters and the problem with oxygen. *Mol. Microbiol. 59*, 1073−82.

(5) Baffert, C., Demuez, M., Cournac, L., Burlat, B., Guigliarelli, B., Bertrand, P., Girbal, L., and Léger, C. (2008) Hydrogen-activating enzymes: Activity does not correlate with oxygen sensitivity. *Angew. Chem., Int. Ed. 47*, 2052−2054.

(6) Liebgott, P.-P., Leroux, F., Burlat, B., Dementin, S., Baffert, C., Lautier, T., Fourmond, V., Ceccaldi, P., Cavazza, C., Meynial-Salles, I., Soucaille, P., Fontecilla-Camps, J. C., Guigliarelli, B., Bertrand, P., Rousset, M., and Léger, C. (2010) Relating diffusion along the substrate tunnel and oxygen sensitivity in hydrogenase. *Nat. Chem. Biol. 6*, 63−70.

(7) Goldet, G., Brandmayr, C., Stripp, S. T., Happe, T., Cavazza, C., Fontecilla-Camps, J. C., and Armstrong, F. A. (2009) Electrochemical kinetic investigations of the reactions of [FeFe]-hydrogenases with carbon monoxide and oxygen: Comparing the importance of gas tunnels and active-site electronic/redox effects. *J. Am. Chem. Soc. 131*, 14979−14989.

(8) Lautier, T., Ezanno, P., Baffert, C., Fourmond, V., Cournac, L., Fontecilla-Camps, J. C., Soucaille, P., Bertrand, P., Meynial-Salles, I., and Leger, C. (2011) The quest for a functional substrate access tunnel in FeFe hydrogenase. *Faraday Discuss. 148*, 385−407.

(9) Stripp, S. T., Goldet, G., Brandmayr, C., Sanganas, O., Vincent, K. A., Haumann, M., Armstrong, F. A., and Happe, T. (2009) How oxygen attacks [FeFe] hydrogenases from photosynthetic organisms. *Proc. Natl. Acad. Sci. U.S.A. 106*, 17331−17336.

(10) Lambertz, C., Leidel, N., Havelius, K. G. V., Noth, J., Chernev, P., Winkler, M., Happe, T., and Haumann, M. (2011) O2-reactions at the six-iron activesite (H-cluster) in [FeFe]-hydrogenase. *J. Biol. Chem. 286*, 40614−40623.

(11) Stiebritz, M. T., and Reiher, M. (2009) Theoretical study of dioxygen induced inhibition of [FeFe]-hydrogenase. *Inorg. Chem. 48*, 7127−7140.

(12) Dogaru, D., Motiu, S., and Gogonea, V. (2009) Inactivation of [Fe-Fe]-hydrogenase by O2. Thermodynamics and frontier molecular orbitals analyses. *Int. J. Quantum Chem. 109*, 876−889.

(13) Dogaru, D., Motiu, S., and Gogonea, V. (2010) Residue mutations in [Fe-Fe]-hydrogenase impedes O2 binding: A QM/MM investigation. *Int. J. Quantum Chem. 110*, 1784−1792.

(14) Bruska, M. K., Stiebritz, M. T., and Reiher, M. (2011) Regioselectivity of H cluster oxidation. *J. Am. Chem. Soc. 133*, 20588−20603.

(15) Baffert, C., Bertini, L., Lautier, T., Greco, C., Sybirna, K., Ezanno, P., Etienne, E., Soucaille, P., Bertrand, P., Bottin, H., Meynial-Salles, I., De Gioia, L., and Léger, C. (2011) CO disrupts the reduced H-cluster of FeFe hydrogenase. A combined DFT and protein film voltammetry study. *J. Am. Chem. Soc. 133*, 2096−2099.

(16) Nicolet, Y., Piras, C., Legrand, P., Hatchikian, C. E., and Fontecilla-Camps, J. C. (1999) Desulfovibrio desulfuricans iron hydrogenase: The structure shows unusual coordination to an active site Fe binuclear center. *Structure 7*, 13−23.

(17) Cohen, J., Kim, K., King, P., Seibert, M., and Schulten, K. (2005) Finding gas diffusion pathways in proteins: Application to O2 and H2 transport in CpI [FeFe]-hydrogenase and the role of packing defects. *Structure 13*, 1321−1329.

(18) Pandey, A. S., Harris, T. V., Giles, L. J., Peters, J. W., and Szilagyi, R. K. (2008) Dithiomethylether as a ligand in the hydrogenase H-cluster. *J. Am. Chem. Soc. 130*, 4533−4540.

(19) King, P., Ghirardi, M., and Seibert, M. Oxygen-resistant hydrogenases and method for designing and making same. U.S. Patent 7501270, filed Apr 16, 2004.

(20) Lemon, B. J., and Peters, J. W. (1999) Binding of exogenously added carbon monoxide at the active site of the iron-only hydrogenase (CpI) from *Clostridium pasteurianum*. *Biochemistry 38*, 12969−12973.

(21) Pereira, A. S., Tavares, P., Moura, I., Moura, J. J. G., and Huynh, B. H. (2001) Mössbauer characterization of the iron−sulfur clusters in *Desulfovibrio vulgaris* hydrogenase. *J. Am. Chem. Soc. 123*, 2771−2782.

(22) Liebgott, P.-P., de Lacey, A. L., Burlat, B., Cournac, L., Richaud, P., Brugna, M., Fernandez, V. M., Guigliarelli, B., Rousset, M., Léger, C., and Dementin, S. (2011) Original design of an oxygen-tolerant [NiFe] hydrogenase: Major effect of a valine-to-cysteine mutation near the active site. *J. Am. Chem. Soc. 133*, 986−997.

(23) Hong, G., Cornish, A. J., Hegg, E. L., and Pachter, R. (2011) On understanding proton transfer to the biocatalytic [Fe—Fe]H subcluster in [Fe—Fe]H2ases: QM/MM MD simulations. *Biochim. Biophys. Acta, Bioenerg. 1807*, 510−517.

(24) Yaffe, E., Fishelovitch, D., Wolfson, H. J., Halperin, D., and Nussinov, R. (2008) MolAxis: Efficient and accurate identification of channels in macromolecules. *Proteins: Struct., Funct., Bioinf. 73*, 72−86.

(25) Travers, M. J., Cowles, D. C., and Ellison, G. B. (1989) Reinvestigation of the electron affinities of molecular oxygen and nitric oxide. *Chem. Phys. Lett. 164*, 449−55.

(26) Lindahl, E., Hess, B., and van der Spoel, D. (2001) GROMACS 3.0: a package for molecular simulation and trajectory analysis. *J. Mol. Model. 7*, 306−317.

(27) Brooks, B. R., Brooks, C. L., Mackerell, A. D., Nilsson, L., Petrella, R. J., Roux, B., Won, Y., Archontis, G., Bartels, C., Boresch, S., Caflisch, A., Caves, L., Cui, Q., Dinner, A. R., Feig, M., Fischer, S., Gao, J., Hodoscek, M., Im, W., Kuczera, K., Lazaridis, T., Ma, J., Ovchinnikov, V., Paci, E., Pastor, R. W., Post, C. B., Pu, J. Z., Schaefer, M., Tidor, B., Venable, R. M., Woodcock, H. L., Wu, X., Yang, W., York, D. M., and Karplus, M. (2009) CHARMM: The biomolecular simulation program. *J. Comput. Chem. 30*, 1545−1614.

(28) Ryde, U., Greco, C., and De, G. L. (2010) Quantum refinement of [FeFe] hydrogenase indicates a dithiomethylamine ligand. *J. Am. Chem. Soc. 132*, 4512−3.

(29) Hess, B., Bekker, H., Berendsen, H. J. C., and Fraaije, J. G. E. M. (1997) LINCS: A linear constraint solver for molecular simulations. *J. Comput. Chem. 18*, 1463−1472.

(30) Zhang, Y., and Skolnick, J. (2005) A protein structural alignment algorithm based on TM-score. *Nucleic Acids Res. 33*, 2302−9.

(31) Humphrey, W., Dalke, A., and Schulten, K. (1996) VMD: Visual molecular dynamics. *J. Mol. Graphics 14*, 33−38.
(32) Becke, A. D. (1988) Density-functional exchange-energy approximation with correct asymptotic behavior. *Phys. Rev. A 38*, 3098.
(33) Perdew, J. P. (1986) Density-functional approximation for the correlation energy of the inhomogeneous electron gas. *Phys. Rev. B 33*, 8822.
(34) Frisch, M. J., Trucks, G. W., Schlegel, H. B. S., Scuseria, G. E., Robb, M. A., Cheeseman, J. R., Scalmani, G., Barone, V., Mennucci, B., Petersson, G. A., Nakatsuji, H., Caricato, M., Li, X., Hratchian, H. P., Izmaylov, A. F., Bloino, J., Zheng, G., Sonnenberg, J. L., Hada, M., Ehara, M., Toyota, K., Fukuda, R., Hasegawa, J., Ishida, M., Nakajima, T., Honda, Y., Kitao, O., Nakai, H., Vreven, T., Montgomery, Jr., J. A., Peralta, J. E., Ogliaro, F., Bearpark, M., Heyd, J. J., Brothers, E., Kudin, K. N., Staroverov, V. N., Kobayashi, R., Normand, J., Raghavachari, K., Rendell, A., Burant, J. C., Iyengar, S. S., Tomasi, J., Cossi, M., Rega, N., Millam, N. J., Klene, M., Knox, J. E., Cross, J. B., Bakken, V., Adamo, C., Jaramillo, J., Gomperts, R., Stratmann, R. E., Yazyev, O., Austin, A. J., Cammi, R., Pomelli, C., Ochterski, J. W., Martin, R. L., Morokuma, K., Zakrzewski, V. G., Voth, G. A., Salvador, P., Dannenberg, J. J., Dapprich, S., Daniels, A. D., Farkas, Ö., Foresman, J. B., Ortiz, J. V., Cioslowski, J., and Fox, D. J. (2009) *Gaussian 09*, Gaussian, Inc., Wallingford, CT.
(35) Singh, U. C., and Kollman, P. A. (1984) An approach to computing electrostatic charges for molecules. *J. Comput. Chem. 5*, 129−145.